Proton spectroscopy beyond the drip line near $A=150$

P. J. Sellin, P. J. Woods, T. Davinson, N. J. Davis, K. Livingston, R. D. Page, and A. C. Shotter
Department of Physics, University of Edinburgh, Edinburgh EH9 3JZ, United Kingdom

S. Hofmann
Gesellschaft für Schwerionenforschung mbH, Darmstadt, Germany

A. N. James
Oliver Lodge Laboratory, University of Liverpool, Liverpool L69 3BX, United Kingdom
(Received 15 January 1993)

The Daresbury recoil separator has been used to measure proton radioactivity from the nuclei ^{150}Lu, ^{151}Lu, and ^{147}Tm, produced using the reactions ^{58}Ni+^{96}Ru→^{154}Hf* and ^{58}Ni+^{92}Mo→^{150}Yb*. The half-life of ^{150}Lu has been measured for the first time as 35±10 ms, which identifies the proton decay as an $l=5$ transition from the $h_{11/2}$ proton state. New half-life and energy measurements have been made for the known proton transitions from ^{147}Tm and ^{151}Lu, which have been unambiguously assigned using the direct mass identification of the recoil separator. A new half-life measurement of the proton emitter ^{109}I is also reported.

PACS number(s): 23.90.+w, 21.10.Pc, 27.70.+q, 27.60.+j

I. INTRODUCTION

Nuclei lying beyond the proton drip line are energetically unbound to proton emission from the nuclear ground state. Measurements of proton emitting nuclei provide unique nuclear structure information for nuclei far from the regions of known data. The sensitivity of the proton partial half-life to the orbital angular momentum of the emitted proton can be used to identify the level ordering of low-lying proton states. At the same time Q_p values derived from measured proton transition energies provide a stringent test of competing mass models in regions far from the known mass surface.

The first examples of direct proton emission were reported in 1982 from the nuclei ^{151}Lu [1] and ^{147}Tm [2]. The proton transition from ^{151}Lu was observed using the in-flight velocity filter SHIP at GSI, whereas the longer-lived ^{147}Tm was initially measured on the GSI on-line mass separator. These two examples formed a region of proton emission from spherical shell-model nuclei and were followed in 1984 by the observation of the deformed transitional proton emitters ^{109}I and ^{113}Cs [3,4]. Further studies of these four nuclei were subsequently carried out using SHIP and a number of weak proton transitions were reported which could not be unambiguously identified [5]. In this paper we report new proton decay half-lives and energy measurements in this region obtained using the Daresbury recoil mass separator and a double-sided silicon strip detector [6,7]. The explicit mass identification provided by this technique has allowed a direct mass assignment to be made in each case.

II. PREVIOUS PROTON RADIOACTIVITY MEASUREMENTS IN THE $A=150$ REGION

During several SHIP experiments the reactions ^{58}Ni+^{92}Mo→^{150}Yb* and ^{58}Ni+^{96}Ru→^{154}Hf* were used to measure proton emission from ^{147}Tm and ^{151}Lu respectively. In each case an intense proton peak was observed, corresponding to the ground-state transitions from ^{147}Tm and ^{151}Lu respectively, plus a number of weaker lines. In general, the assignment of the parent nucleus for each observed transition was achieved using excitation function systematics and Q_p value arguments. In the case of the reaction ^{58}Ni+^{92}Mo→^{150}Yb* the ground-state peak from ^{147}Tm was clearly seen with an energy $E_p \simeq 1.05$ MeV. The half-life of this transition had been previously measured at the GSI mass separator with a value of 560±40 ms [2], identifying the $h_{11/2}$ proton level as the origin of the transition. In the SHIP experiments a weaker line was also observed at 1118 keV, which was tentatively assigned to proton emission from a low-lying state in ^{147}Tm [8]. The compound nucleus excitation energy used in this reaction was 42 MeV, which corresponds to the maximum cross section of both the two-nucleon channels (^{148}Er, ^{148}Tm, and ^{148}Yb) and the low-lying excited states of the three-nucleon channels. For such nuclei lying beyond the known mass surface, Q_p values can be predicted using a mass model such as that of Möller and Nix [9]. These Q_p value estimates identified ^{147}Tm as the most likely origin of this weaker transition, although proton emission from an isomeric state in ^{148}Tm could not be ruled out. The measured half-life of this transition was 360±80 μs [8], which is consistent with an $l=2$ rather than an $l=0$ transition. Four additional lines were also observed in this reaction with energies of 2467±20 keV, 2851±15 keV [5,10], 2935 and 3277 keV [11], and with half-lives in the range 1 μs–10 ms. This upper limit on the half-life rules out β-delayed proton emission as a source of these lines. No assignments were suggested for these lines and until this work no further experiments had been performed to reproduce them.

Proton emission from ^{151}Lu was convincingly identified

at SHIP using the reaction $^{58}Ni+^{96}Ru\rightarrow^{154}Hf^*$ which produced a proton peak at an energy of 1.233 MeV. The measured half-life of 85 ± 10 ms also identified this decay as an $l=5$ transition from the $h_{11/2}$ proton level. In addition, a weak transition was observed at an energy of 1263 keV from the same reaction, produced at excitation energies in the range 72–78 MeV. The most likely source of this transition was from a high-spin ground state $l\geq5$ level in ^{150}Lu. The excitation energies used to produce this line were higher than that for the peak cross section of the ^{151}Lu transition, consistent with moving from a three-nucleon ($p2n$) to a four-nucleon ($p3n$) evaporation channel. In an alternative explanation suggested by Hofmann [5] the 1263-keV line could originate from a low-spin isomeric state in ^{151}Lu, fed via β decay from ^{151}Hf. Production of ^{151}Hf via the $3n$ channel might account for the higher excitation energy required, relative to direct production of ^{151}Lu via the $p2n$ channel. As the ground state of ^{151}Lu would also be populated in the same way from ^{151}Hf, this would explain the observation at SHIP of both the 1263-keV line and the ^{151}Lu line at the higher excitation energy. The calculated Wentzel-Kramers-Brillouin (WKB) proton half-life for a 1.26-MeV transition is approximately 40 ms for an $l=5$ transition from ^{150}Lu, whereas the β half-life of ^{151}Hf is estimated to be in the range 100–300 ms. The low statistics of the SHIP measurement prevented a half-life from being obtained, giving only an experimentally deduced lower limit of 10 ms which leaves either mechanism as a possibility. Furthermore, an additional weak line was seen from this reaction ($E_x=68$ MeV) with an energy of 1360 ± 10 keV [5]. Decay energy spectra from this experiment [11] show this peak barely identifiable above background and with an experimentally deduced lower half-life limit of 2 ms. No assignment was given for this transition.

The aim of this work was therefore to identify proton transitions produced from the reactions $^{58}Ni+^{92}Mo\rightarrow^{150}Yb^*$ and $^{58}Ni+^{96}Ru\rightarrow^{154}Hf^*$, exploiting the greater sensitivity and explicit mass identification of the Daresbury technique (see Sec. III). This method has already been successfully used to identify the new odd-odd proton emitters ^{156}Ta and ^{160}Re [12].

III. EXPERIMENTAL TECHNIQUE

The evaporation residue implantation detection system [6,7] has been developed on the Daresbury recoil mass separator as a highly sensitive technique for the measurement of short-lived (≥1 μs) low cross section proton-emitting nuclei. The technique offers a number of advantages over the previous SHIP experiments, namely, the explicit mass identification and the increased sensitivity to low cross section decay lines. This has made possible the study of proton transitions from evaporation residues produced via the $p3n$ channel, such as ^{160}Re. The recoil separator provides fast in-flight separation of the beam-like particles from the evaporation residues, which are dispersed horizontally at the separator focal plane according to their A/Q (mass to ionic charge state ratio). The residues are implanted into the double-sided silicon strip detector located at the focal plane and an explicit mass identification is made from the horizontal position of each implantation event in the detector. In this way an indirect mass assignment using excitation functions can be avoided.

The strip detector records the x,y position and energy of each implantation event and of the subsequent proton and alpha decays. The detector consists of 48 strips per face, orthogonally crossed to provide two-dimensional position information. Each face has a strip pitch of 335 μm with an active area of 16 mm$\times$16 mm and a thickness of 60–110 μm. The excellent position resolution enables efficient position and time correlations to be made between implantation events and their causally related decays, which produces extremely clean decay energy spectra for transitions over a long range of decay half-lives.

A rotating aperture wheel containing degrading foils and collimating masks is positioned immediately in front of the strip detector. The aluminum foils reduce the energy of the residues before implantation into the detector and have a range of thicknesses from 200 μg cm^{-2} to 2 mg cm^{-2}. This energy reduction minimizes the saturation of the high gain decay event amplifiers caused by implantation events. The strip detector is mounted in front of a passivated implanted planar silicon detector with an active area of 450 mm^2 and a thickness of 700 μm. This detector is used to measure the energies of positrons, x rays, low-energy γ rays, and β-delayed protons in coincidence with events in the strip detector.

Two consecutive runs were performed on the Daresbury recoil separator over a period of 72 h, using the reactions $^{58}Ni+^{92}Mo\rightarrow^{150}Yb^*$ and $^{58}Ni+^{96}Ru\rightarrow^{154}Hf^*$. For the first reaction 500 μg cm^{-2} thick self-supporting foils of isotopically enriched ^{92}Mo were irradiated with a beam of ^{58}Ni ions at an energy of 261 MeV. This produced the compound nucleus $^{150}Yb^*$ with a mean excitation energy of $\simeq50$ MeV which was chosen to maximize the yield of ^{147}Tm produced via the $p2n$ evaporation channel. The second reaction used 400 μg cm^2 thick foils of isotopically enriched ^{96}Ru mounted on foils of 700 μg cm^{-2} thick aluminum with beam energies of 300 and 311 MeV, producing the compound nucleus $^{154}Hf^*$ with mean excitation energies of $\simeq61$ and $\simeq69$ MeV respectively, which were designed to optimize the production of ^{150}Lu via the $p3n$ channel. The ^{96}Ru targets were mounted onto the target ladder with the aluminum "backing" facing the beam in order to prevent additional scattering of the evaporation residues from the aluminum, so maximizing their acceptance by the recoil separator.

In the first reaction the recoil separator was set to position $A=147$ evaporation residues onto the center of the detector, with charge state $Q=27^+$. The beam current was maintained at approximately 5 particles nA over a total period of 36 h, with an average implantation rate of 700 Hz. In the second reaction the recoil separator was adjusted to position $A=150$ residues onto the center of the detector, with charge state $Q=29^+$. An implantation rate of 1.5 kHz was maintained over a period of 24 h with a beam energy of 300 MeV, followed by a further 8 h with a beam energy of 311 MeV.

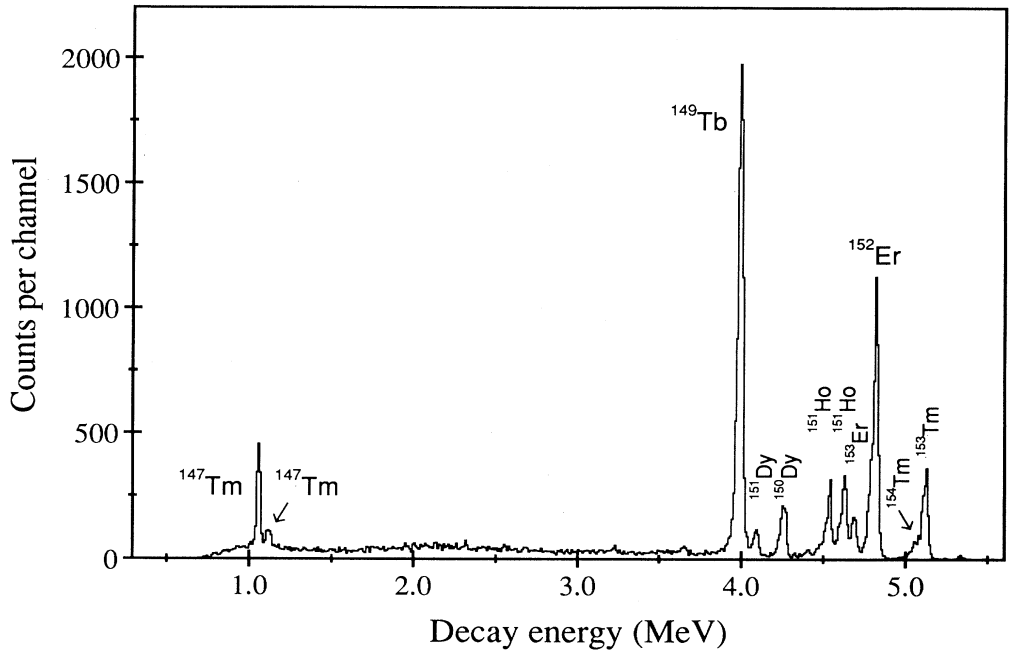

FIG. 1. Decay energy spectrum for all events from ^{150}Yb*. The two proton peaks from ^{147}Tm are clearly visible at energies just above 1.0 MeV, and a variety of alpha peaks are present at higher energies.

IV. RESULTS

A. Proton emission from ^{147}Tm

The decay energy spectrum observed from the reaction ^{58}Ni+^{92}Mo$\rightarrow$^{150}Yb* is shown in Fig. 1 with two proton peaks clearly visible at energies just above 1 MeV. The more intense peak at an energy of 1.05 MeV is identified as the proton decay of the ground state of ^{147}Tm. The weaker proton peak has a measured energy of 1.11 MeV and a cross section of 5 μb, deduced assuming a measured cross section of 30 μb for the ground-state peak [5]. The two proton peaks are clearly resolved, with an energy resolution of 25 keV FWHM. A number of intense alpha peaks also occur within a range of energies from 3.9 to 5.3 MeV, produced from nuclei with mass numbers in the range $A=150-154$ originating from isotopic contaminants in the target.

Figure 2 shows the decay energy plotted against the mass of the evaporation residue ($Q=27^+$). The alpha lines visible at high energies mostly reach the separator focal plane as charge state ambiguities ($Q=28^+$). The resulting mass distribution for these residues is displaced from the main $Q=27^+$ distribution by about half a mass unit. The strong line visible at approximately 1.0 MeV in the $A=147$ region contains the two proton peaks from ^{147}Tm, which are not resolved in this spectrum. Consequently, the 1.11-MeV peak is assigned to the proton decay of an $A=147$ nucleus, which, based on the Q value arguments discussed earlier, is therefore identified as proton emission from an excited state in ^{147}Tm. The energy of this transition was measured from the data using the ground state ^{147}Tm peak and the ^{151}Ho, ^{151}Ho^m alpha peaks [13] as calibration points. The proton energy of the ground state ^{147}Tm transition has been measured by Hofmann at SHIP using the alpha lines from ^{151}Ho, ^{151}Ho^m, and ^{152}Er plus the proton line from ^{151}Lu as calibration energies. Our measurement of the excited-state transition in ^{147}Tm is $E_p=1110.8\pm3.9$ keV, after correcting for the energy deficit of protons in silicon [5] and the deficit-corrected recoil energy of the daughter nucleus [14]. This measurement is consistent with the previously measured value of 1118.5 ± 5.3 keV [5] and has an im-

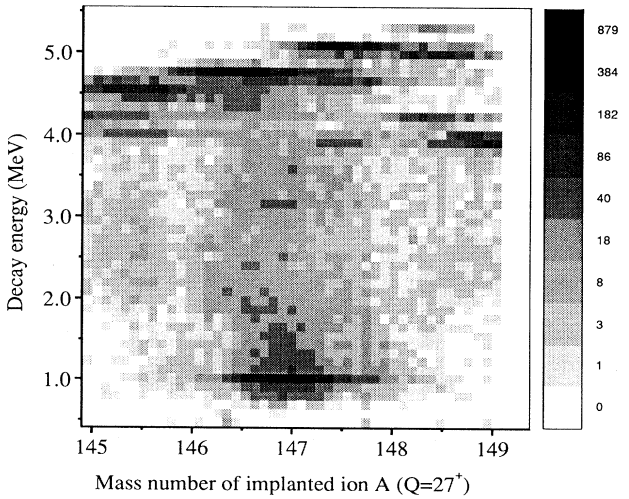

FIG. 2. Plot of decay energy vs mass number of the implanted ion, for events from ^{150}Yb*. The two proton peaks are contained within the low-energy line in mass group $A=147$.

proved precision which is mainly due to the good peak/background ratio contained in this data.

Figure 3 shows a sequence of mass gated $A=147$ decay energy spectra expanded about the two proton peaks. The four spectra show decay events back-correlated to a preceding implantation event within the given implantation-decay time difference. The change in relative intensity of the two proton peaks with increasing time difference is clearly shown in the spectra, which is due to the peaks' different half-lives. The 10-ms time difference spectrum contains all the yield of the 1.11-MeV peak whereas the intensity of the 1.05-MeV peak increases through the sequence of spectra. Figure 4 shows the implantation-decay time difference spectra for the 1.11-MeV peak and the 1.05-MeV peak from which new independent half-life measurements have been made for each of the two lines. The resulting half-life values, deduced from least-squares fits to the data, are $t_{1/2}=360\pm40$ μs for the excited-state transition (previous value $t_{1/2}=360\pm80$ μs [8]) and $t_{1/2}=580\pm70$ ms for the ground-state transition (previous value $t_{1/2}=560\pm40$ ms [15]) which are in excellent agreement with the previous measurements.

Tentative evidence has also been discovered for a previously unidentified weakly populated ($\sigma<100$ nb) proton decay peak in the $A=147$ mass gated spectrum with an energy of 947.4±5.0 keV and a half-life in the range 100 μs–10 ms. On the basis of Q_p-value arguments the most likely source of this activity is ^{147}Tm, since for the remaining $A=147$ residues typical Q_p values are -0.4, -2.1, and -0.3 MeV for ^{147}Yb, ^{147}Er, and ^{147}Ho, respectively [9]. However, further data will be required before a positive assignment can be made.

No evidence was seen for the four higher-energy short-lived peaks observed by Hofmann *et al.* from ^{150}Yb*, despite using the same beam energy as the GSI measurements. These peaks appeared in the GSI data [11] with energies of approximately 2467 keV ($\sigma=10$ μb), 2851 keV ($\sigma=20$ μb), 2935 keV ($\sigma=5$ μb), and 3277 keV ($\sigma=5$ μb). Figure 5 shows the position-correlated decay energy spectrum from the present data within a 50-ms implantation-decay time gate. There is no evidence for any peaks above the background events at any energy between that of the ^{147}Tm peaks and the alpha peak from

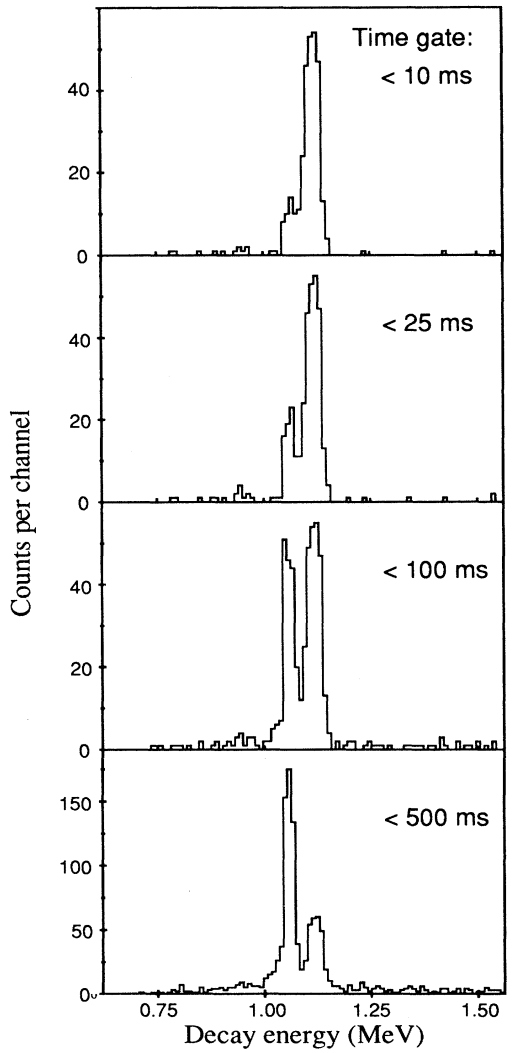

FIG. 3. Sequence of $A=147$ position-correlated decay energy spectra showing the two intense proton peaks from ^{147}Tm, gated on increasing implantation-decay time difference.

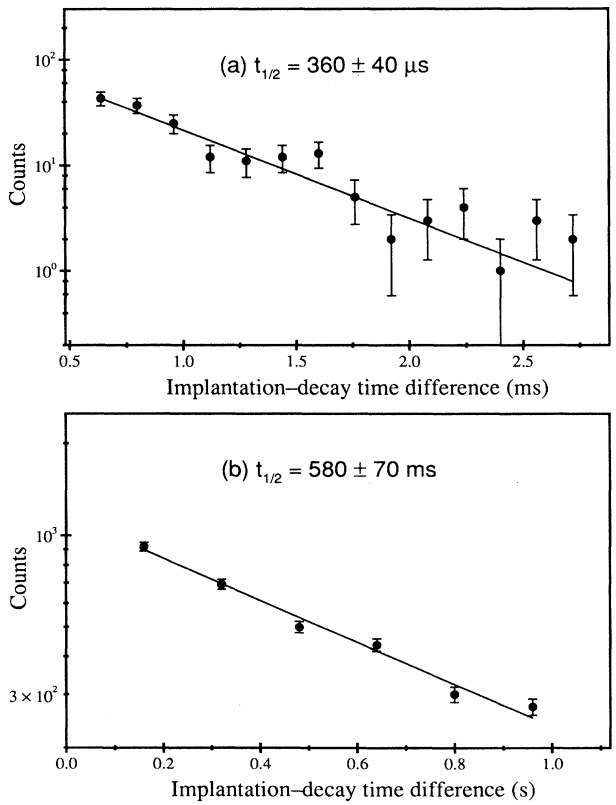

FIG. 4. Implantation-decay time difference spectra for (a) the 1.11-MeV ^{147}Tm proton transition and (b) the ground-state 1.05-MeV ^{147}Tm proton transition. Also shown are least-squares fits to the data, with the measured half-lives.

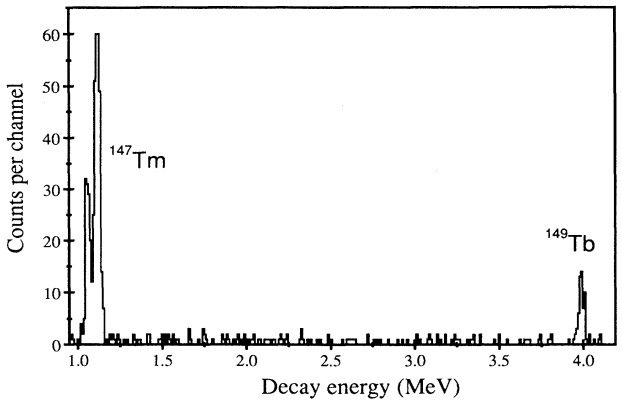

FIG. 5. Energy spectra for time gated (<50 ms) decay events from all mass groups for the reaction ^{58}Ni+^{92}Mo$\rightarrow$^{150}Yb*. No evidence was found for the discrete peaks seen at GSI at energies between 2.5 and 3.5 MeV.

^{149}Tb at 3.99 MeV. Based on the GSI data such peaks would be expected to occur in this spectrum with yields of between 10 and 50 counts. In the present data the presence of $Q=28^{+}$ residues means that the recoil separator accepts masses over a continuous range from $A=145$ to 154 and it is therefore possible to exclude as the source of this activity nuclei in this mass range. The origin of the peaks in the GSI data therefore remains unknown.

B. Proton emission from ^{150}Lu

Figure 6 shows the decay energy spectrum for all events from the reaction ^{58}Ni+^{96}Ru$\rightarrow$^{154}Hf*. A variety of intense alpha lines are present, produced mainly from isotopic contamination of the target. The proton peak from ^{151}Lu is clearly visible at an energy of 1.23 MeV and contains a slight asymmetry on the high-energy side. The detailed mass and energy structure of this line can be identified in Fig. 7 which shows three mass gated spectra containing position-correlated decay events within a 50-ms implantation-decay time gate. Figure 7(a) is mass gated on both $A=150$ and 151, and clearly shows the higher-energy component on the side of the 1.23-MeV peak. Figure 7(b) is gated on $A=151$ and shows the 1.23-MeV proton peak from ^{151}Lu without the higher-energy component. This mass gated spectrum provides the first direct mass assignment of the 1.23-MeV transition to ^{151}Lu. Figure 7(c) is gated on $A=150$ and clearly shows the weaker proton peak at an energy of 1.26 MeV. This transition is therefore unambiguously assigned to proton emission from an $A=150$ nucleus. Among the $A=150$ evaporation residues only ^{150}Lu has a positive predicted Q_p value which is in agreement with the measured value, although emission of an $h_{11/2}$ proton could, in principle, occur from long-lived $\pi h_{11/2}\nu h_{11/2}^{-1}10^{+}$ isomeric states such as those measured in the $N=81$ isotones ^{146}Tb, ^{148}Ho, and ^{150}Tm. However, the half-life of this isomer in ^{150}Tm is $t_{1/2}=5.2\pm0.3$ ms [16] and can be excluded as a source of this activity. In addition, the predicted Q_p value for proton emission from the 10^{+} state in ^{150}Tm to the corresponding $\nu h_{11/2}^{-1}$ state in ^{149}Er is only $\simeq$300 keV. The assignment of this proton transition to the $p3n$ evaporation channel from ^{154}Hf* is also consistent with the observed yield and we therefore identify the 1.26-MeV peak as proton emission from ^{150}Lu.

The energy of the ^{150}Lu peak was measured from this

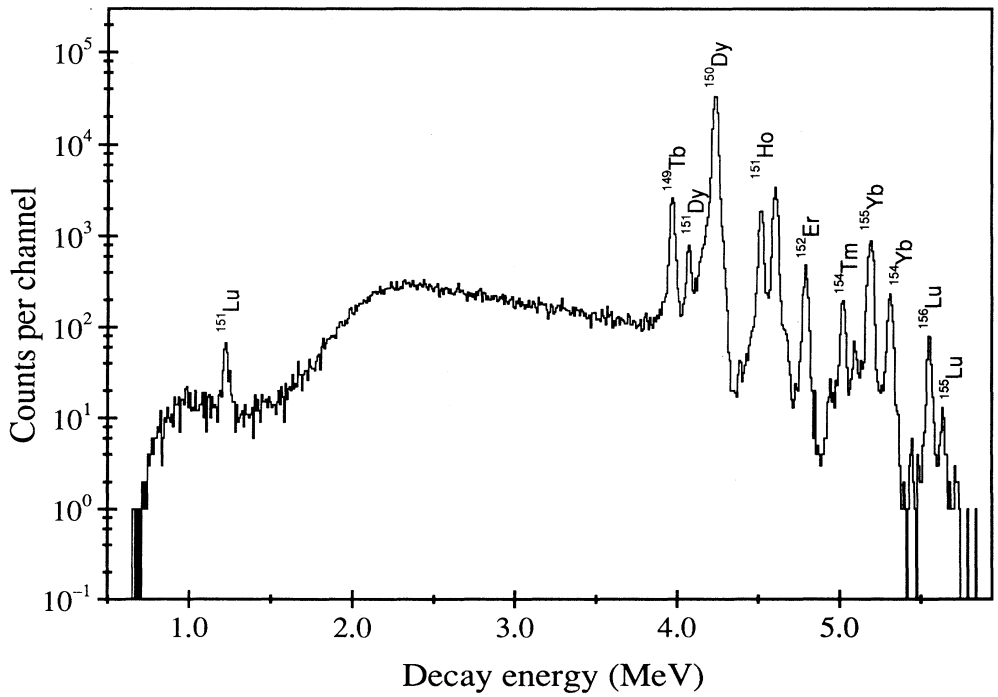

FIG. 6. Decay energy spectrum for all events from ^{154}Hf*. The proton peak from ^{151}Lu is clearly visible at an energy of 1.23 MeV.

data, using the proton peak from ^{151}Lu and the alpha peaks from ^{151}Ho, ^{151}Ho^{m} as calibration energies. The transition energy obtained after corrections was $E_p = 1261.0 \pm 4.0$ keV, which is in excellent agreement with the previously measured value of 1262.7 ± 3.6 keV [5]. Figure 8 shows the time difference spectra obtained for ^{150}Lu and ^{151}Lu and their measured half-lives, giving a first half-life measurement of ^{150}Lu with a value of $t_{1/2} = 35 \pm 10$ ms (previous limit > 10 ms [8]). The half-life was also measured for ^{151}Lu giving $t_{1/2} = 90 \pm 10$ ms which is in good agreement with the previous value ($t_{1/2} = 85 \pm 10$ ms [8]).

No evidence was found from this reaction for the weak 1.36-MeV proton line tentatively reported by Hofmann *et al.* The GSI data suggest a very weak peak at 1.36 MeV with an approximate cross section of 1 μb and a lower half-life limit of 2 ms. By comparison with the yield of the ^{150}Lu peak, the present data would be expected to contain approximately 10 counts at 1.36 MeV. The decay energy spectra from our data show no evidence in any mass group for a peak at this energy. Due to the poor event statistics in the GSI spectrum, it must be concluded that the suggested peak is actually due to statistical fluctuations in the event background.

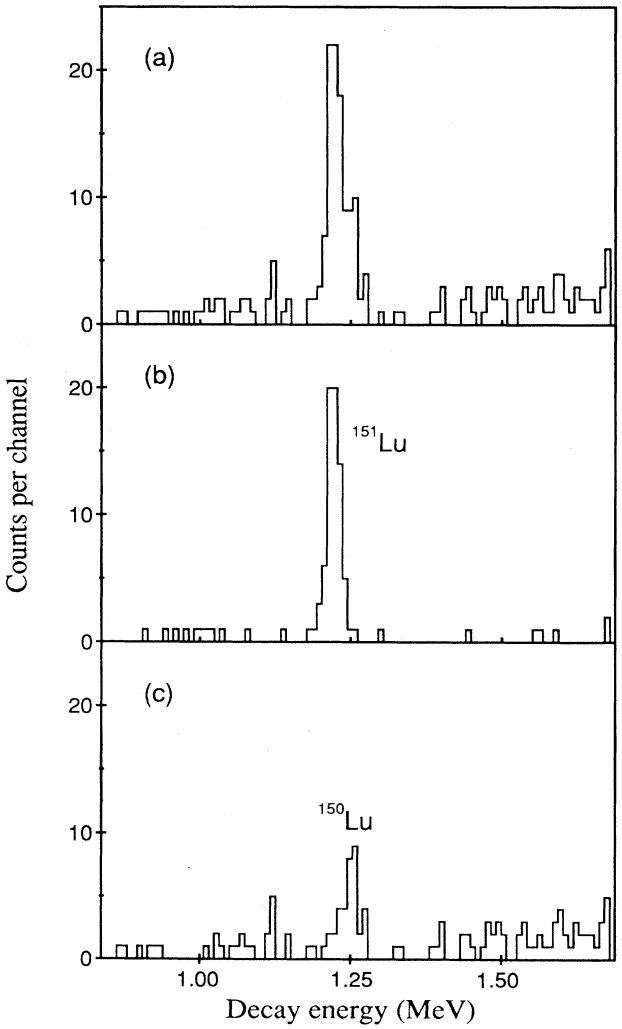

FIG. 7. Mass gated energy spectra showing proton peaks from ^{154}Hf* time gated within 50 ms. (a) Spectrum gated around both $A = 150$ and 151. (b) Spectrum gated around $A = 151$ showing the 1.23-MeV proton peak from ^{151}Lu. (c) Spectrum gated around $A = 150$ showing the weaker 1.26-MeV proton peak, assigned to the decay of ^{150}Lu.

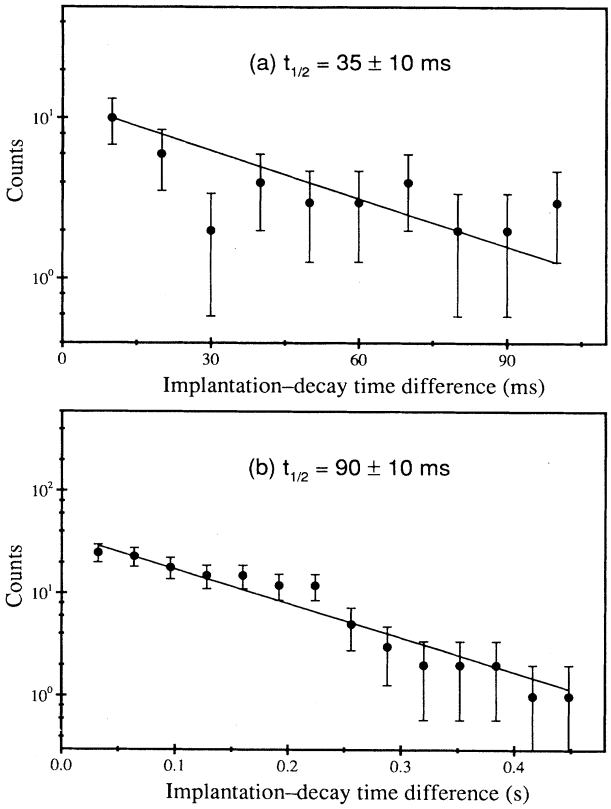

FIG. 8. Implantation-decay time difference spectra for (a) ^{150}Lu and (b) ^{151}Lu. Also shown are least-squares fits to the data, with measured half-lives.

TABLE I. Summary and comparison of proton decay half-life and energy measurements from this work.

Nucleus	New E_p (keV)	Previous E_p [a] (keV)	New $t_{1/2}^{expt}$	Previous $t_{1/2}^{expt}$
^{147}Tm		1051.0±3.3	580±70 ms	560±40 ms[b]
^{147}Tm	1110.8±3.9	1118.5±5.3	360±40 μs	360±80 μs[c]
^{150}Lu	1261.0±4.0	1262.7±3.6	35±10 ms	$\geq$ 10 ms[c]
^{151}Lu		1232.8±2.8	90±10 ms	85±10 ms[c]
^{109}I		812.6±4.0	100±5 μs	107±6 μs[d]

[a] Hofmann [5].
[b] Larsson *et al.* [15].
[c] Hofmann *et al.* [8].
[d] Heine *et al.* [17].

The proton transitions measured in this work have been assigned to proton emission from the nuclei ^{147}Tm, ^{150}Lu, and ^{151}Lu. The new proton energies and half-lives are summarized in Table I, together with a new half-life value for the proton emitter ^{109}I which was measured during a preliminary experiment. Previous energy and half-life measurements are also shown in Table I. The present half-life measurements are consistent with the previously recorded values and have a comparable or improved precision.

V. DISCUSSION

A. Assignment of the proton transitions from ^{147}Tm

A comparison of the measured proton half-lives with calculated estimates allows the orbital angular momentum of the emitted proton to be identified. In the shell-model nuclei in this region the proton single-particle levels $s_{1/2}$, $d_{3/2}$, and $h_{11/2}$ are all candidates to occupy the Fermi level and their relative ordering is generally uncertain. Table II summarizes the results of half-life estimates for the measured proton transitions from ^{147}Tm, calculated using the WKB approximation with the optical-model potential of Becchetti and Greenlees [18]. Similar half-life values are calculated using the potential of Perey [19] and, in general, the variations in half-life due to the choice of potential are not significant in comparison with the sensitivity of the half-life to the proton l value. The existing assignment of the 1.051-MeV ^{147}Tm peak to an $l=5$ transition from an $h_{11/2}$ orbital is clearly confirmed by this half-life measurement. In the case of the 1.111-MeV excited-state transition from ^{147}Tm, the new half-life measurement provides further evidence to support an $l=2$ proton transition and we therefore assign this activity to proton emission from the $d_{3/2}$ state, lying at an energy of 60 keV above the $h_{11/2}$ ground state (see Fig. 9). This is in contrast to some previous authors (e.g., [20–22]) who have assumed an $s_{1/2}$ proton level for this excited state.

The energy systematics of the $d_{3/2}$ and $s_{1/2}$ levels in even-N thulium isotopes above $N=82$ [22,23] show the $s_{1/2}$ level occupying the first excited state with an excitation energy of approximately 40 keV. The $d_{3/2}$ level in ^{153}Tm lies above the $s_{1/2}$ level with an excitation energy of 135 keV above the $h_{11/2}$ ground state [21]. In ^{151}Tm the sequence of gamma transitions between low-lying single-particle states ($g_{7/2}$-$s_{1/2}$) has been observed [24,22] although no measurement has been made of the $s_{1/2}$ excitation energy above the $h_{11/2}$ ground state. Below $N=82$ no states are known in ^{149}Tm apart from the $h_{11/2}$ ground state [25] and for ^{147}Tm the only known level assignments are from proton radioactivity experiments. The energy of the $s_{1/2}$ level in ^{151}Tm was deduced by Akovali *et al.* [22] by interpolating between the 43-keV $s_{1/2}$ state in ^{153}Tm and the 60-keV proton-emitting state in ^{147}Tm, which was assumed to be $s_{1/2}$. Our assignment of the $d_{3/2}$ state as the first excited level in ^{147}Tm therefore casts doubt on these published absolute excitation energies of the single-particle states in ^{151}Tm. Further-

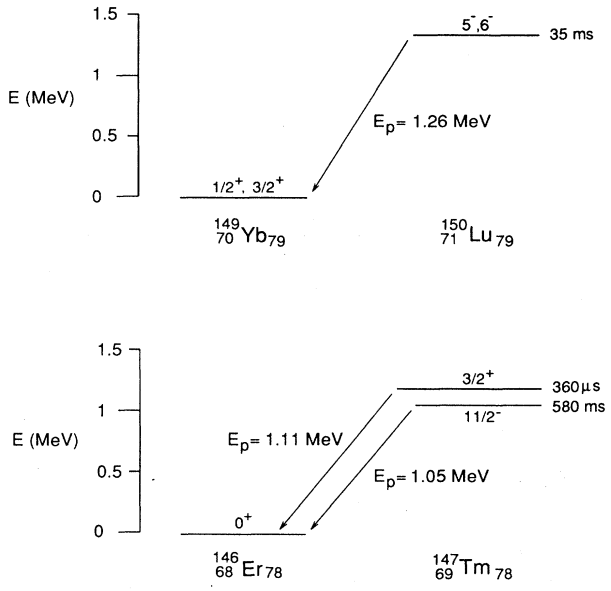

FIG. 9. Deduced partial level schemes of ^{150}Lu and ^{147}Tm showing the measured direct proton transitions.

TABLE II. Summary of calculated half-lives for the measured proton transitions.

Nucleus	^{147}Tm	^{147}Tm	^{150}Lu	^{151}Lu
E_p (keV)	1051.0±3.3	1110.8±3.9	1261.0±4.0	1232.8±2.8
Q_p (keV)[a]	1071.3±3.3	1131.5±3.9	1283.2±4.0	1254.7±2.8
Measured half-life $t_{1/2}^{expt}$	580±70 ms	360±40 μs	35±10 ms	90±10 ms
Proton branch b_p	21±10 %[b]	≃100%[c]	80±20 %[c]	70±35 %[c]
Partial half-life $t_{1/2,p}^{expt}$	$2.8^{+3.1}_{-1.2}$ s	360±40 μs	40^{+30}_{-20} ms	130^{+160}_{-50} ms
$t_{1/2,p}^{calc}$[d] $3s_{1/2}$	95 μs	17 μs	1.4 μs	2.8 μs
$2d_{3/2}$	860 μs	150 μs	13 μs	24 μs
$1h_{11/2}$	2.7 s	460 ms	33 ms	62 ms

[a] $Q_p = E_p$ + recoil energy of nucleus + screening correction estimated from [32].
[b] b_p from [15].
[c] b_p deduced using β-decay half-life estimates from [31].
[d] WKB calculations [33] using the Becchetti-Greenlees potential, assuming a spectroscopic factor of unity.

more, the positioning of the $d_{3/2}$ state beneath the $s_{1/2}$ state in odd-even nuclei below $N=82$ has been recently suggested by the measurement of proton states in ^{145}Tb [26].

B. The proton decay of ^{150}Lu

A comparison between the calculated and measured proton partial half-lives for ^{150}Lu and ^{151}Lu is also given in Table II, covering the $s_{1/2}$, $d_{3/2}$, and $h_{11/2}$ proton states. Partial proton half-lives are calculated as before using the WKB approximation with the real part of the optical-model potential from Becchetti and Greenlees. For both ^{150}Lu and ^{151}Lu the new half-life measurements clearly identify an $l=5$ transition in each case and exclude the emission of either an $l=0$ or 2 proton.

Odd-odd nuclei in this region with $N=79$ or 81 have two β-decaying states which lie very close together in energy. The high-spin state has $J^{\pi}=5^-$ or 6^- produced by the coupling of an $h_{11/2}$ proton and an $s_{1/2}$ or $d_{3/2}$ neutron hole, whilst the low-spin state has $J^{\pi}=1^+$ produced by the coupling of $s_{1/2}$ or $d_{3/2}$ protons with neutron holes. The high-spin level has been assigned to a 6^- state in the $N=79$ nucleus ^{148}Tm [27] and in the $N=81$ nuclei ^{148}Ho [28] and ^{150}Tm [27,29]. The relative separation of the two levels in this region is generally unknown, although Nitschke *et al.* [30] place the 6^- state in ^{148}Ho and ^{150}Tm approximately 100 keV above the 1^+ ground state. The negative-parity high-spin states are preferentially populated when these odd-N nuclei are produced via heavy-ion fusion-evaporation reactions, whereas only the 1^+ state is observed when produced from a β-decaying precursor.

The observed $l=5$ 1.26-MeV proton transition is assigned to proton emission from the high-spin 5^- or 6^- level in ^{150}Lu to a low-spin (probably either $s_{1/2}$ or $d_{3/2}$) neutron hole state in ^{149}Yb and is shown in Fig. 9. This is consistent with the high-spin level occupying either the ground state or low-lying isomeric state in ^{150}Lu and continues the trend of $l=5$ proton emission from $h_{11/2}$ proton states in ^{151}Lu and ^{147}Tm. Following the recent discovery of proton radioactivity from ^{156}Ta and ^{160}Re, the observed proton emission from ^{150}Lu completes a sequence of three consecutive odd-odd proton emitters, where below $N=82$ proton emission is seen from the $h_{11/2}$ proton orbital and above $N=82$ from the $d_{3/2}$ proton orbital.

C. Half-life predictions

Drip line proton radioactivity has been established from nuclei in two distinct regions of the nuclear chart. Between $Z=53-55$ proton emission has been identified from the deformed transitional nuclei ^{109}I and ^{113}Cs, whereas the remaining examples occur from spherical nuclei between $Z=69-75$ and with neutron numbers near 82. As the available data on proton transition half-lives increase, it is of interest to compare the measured values for nuclei from both regions with the various available calculations.

Calculated proton decay half-lives are shown in Table III, produced using a selection of theoretical approaches. Two sets of half-lives are shown calculated using the WKB approximation and the real part of the optical-model potential, with the parameters of Becchetti and

TABLE III. Summary of proton partial half-lives for the known drip line proton transitions, compared to various calculated values.

Nucleus	Q_p[a] (keV)	$t_{1/2,p}^{expt}$[e]	l	$t_{1/2,p}^{calc}$[f] B+G[g]	Perey[g]	Bugrov[h]
^{160}Re[b]	1284±6	870±200 μs	2	160 μs	130 μs	
^{156}Ta[b]	1042±13	165^{+165}_{-55}	2	42 ms	32 ms	
^{151}Lu	1254.7±2.8	130^{+160}_{-50} ms	5	62 ms	24 ms	
^{150}Lu	1283.2±4.0	40^{+30}_{-20} ms	5	33 ms	13 ms	
^{147}Tm	1071.3±3.3	$2.8^{+3.1}_{-1.2}$ s	5	2.7 s	1.0 s	
^{147}Tm	1131.5±3.9	360±40 μs	2	150 μs	120 μs	
^{113}Cs	977.1±3.7[c]	33±7 μs[d]	4	140 μs	110 μs	29–41 μs[i]
			2	0.4 μs	0.3 μs	0.4–6.8 μs[j]
^{109}I	828.9±4.0[c]	100±5 μs	4	3.0 ms	2.5 ms	2.3–2.8 ms[k]
			2	7.3 μs	5.7 μs	30–190 μs[l]

[a] $Q_p = E_p$ + recoil energy of nucleus + screening correction estimated from [32].
[b] From Page *et al.* [12].
[c] From Hofmann [5].
[d] From Gillitzer *et al.* [4].
[e] Experimental proton partial half-life $t_{1/2,p}^{expt}$ deduced from the measured proton transition half-life and the calculated β partial half-life [31].
[f] Calculated proton partial half-life $t_{1/2,p}^{calc}$, assuming a spectroscopic factor of unity.
[g] WKB calculations [33]: BG, Becchetti-Greenlees potential [18], Perey, Perey potential [19].
[h] Half-lives are calculated using a deformed potential [35], with the quantum numbers noted below:
[i] $\beta_2 \simeq 0.10-0.15, \frac{3}{2}^+$ [421].
[j] $\beta_2 \simeq 0.10-0.15, \frac{1}{2}^+$ [420].
[k] $\beta_2 \simeq 0.05-0.10, \frac{3}{2}^+$ [421].
[l] $\beta_2 \simeq 0.05-0.10, \frac{1}{2}^+$ [420].

Greenlees [18] and of Perey [19]. The potential of Becchetti and Greenlees is derived from proton scattering data taken at proton energies of 30–40 MeV whilst the potential of Perey provides an alternative parameter set for proton energies below 20 MeV [34]. In addition, Table III shows half-lives for ^{109}I and ^{113}Cs calculated using the multiparticle model of Bugrov and Kadmenskiĭ [35] which are calculated using an axially deformed Woods-Saxon potential.

Nuclei close to the $N=82$ shell closure are generally spherical in shape, and proton half-lives measured from ^{147}Tm, ^{150}Lu, and ^{151}Lu are expected to be described well by transitions between shell-model states. Since for this region proton emission enhancement factors are not expected, it is possible to exclude any calculated half-lives which are significantly longer than the measured values. The calculated half-lives shown in Table III are either in agreement with or are shorter than the measured values. Half-lives calculated using the Becchetti and Greenlees potential are consistently longer than those produced using the potential of Perey and are in better agreement with the data. The largest discrepancy using the Becchetti and Greenlees potential is for ^{160}Re where the calculated half-life is within a factor of 5 of the measured value. It can be concluded therefore that these transitions are consistent with a spherical shell-model description of these nuclei. However, the position is different for the two lighter nuclei ^{109}I and ^{113}Cs. The predicted shell-model states around the Fermi level in these nuclei are the $2d_{5/2}$ and $1g_{7/2}$ levels, above the ^{100}Sn core. In both nuclei the calculated half-lives for $l=4$ transitions between shell-model states are longer than the measured values, particularly in the case of ^{109}I, and hence can be excluded. For $l=2$ transitions hindrance factors of up to $20\times$ for ^{109}I and $100\times$ for ^{113}Cs are required to give agreement between the calculated shell-model half-lives and the data. This apparent failure of the shell-model description is not unexpected since both ^{109}I and ^{113}Cs are predicted to exhibit substantial prolate deformation [9,36], typically $\beta_2 \simeq 0.15-0.20$ for ^{109}I and $\beta_2 \simeq 0.20-0.25$ for ^{113}Cs. In contrast, the deformation dependent model of Bugrov and Kadmenskiĭ [35] calculates half-lives for ^{109}I and ^{113}Cs which are in good agreement with the measured values. The half-lives given in Table III use the deformation values $\beta_2 \simeq 0.05-0.10$ for ^{109}I and $\beta_2 \simeq 0.10-0.15$ for ^{113}Cs to obtain the best fit to the experimental half-lives, and Bugrov and Kadmenskiĭ assign the transitions to the Nilsson orbitals $\frac{1}{2}^+[420]$ and $\frac{3}{2}^+[421]$, respectively. Clearly it would be desirable to test the general validity of the Bugrov model by measuring proton transitions in the intermediate region of highly deformed light rare-earth nuclei.

D. Mass model predictions

The observation of proton emission from ^{150}Lu and ^{151}Lu establishes the first pair of adjacent proton-emitting isotopes. It is therefore of interest to compare the proton decay energies for ^{150}Lu and ^{151}Lu with calculated values from a selection of mass models. Figure 10 shows Q_p values calculated using the macroscopic-microscopic model of Möller and Nix [9], the spherical shell-model calculations of Liran and Zeldes [37] and the droplet model of Myers [38]. The experimentally measured Q_p values for ^{150}Lu and ^{151}Lu are shown, together with the only other known Q_p value derived from mass measurements. It can be seen that the proton emission data produce Q_p values for nuclei lying eight isotopes beyond the known mass surface. Despite this both the mass models of Möller and Nix and of Liran and Zeldes fit the proton emission values to within approximately 200 keV. However, the strength of the odd-even staggering in the Möller and Nix calculations is greater than in the data, in contrast to the Liran and Zeldes values which underestimate this effect. The Myers' liquid drop calculations are consistently lower than the actual Q_p values by about 700 keV, which is a known feature of this model [39] and is also seen in the neutron-deficient thulium, tantalum, and rhenium isotopes.

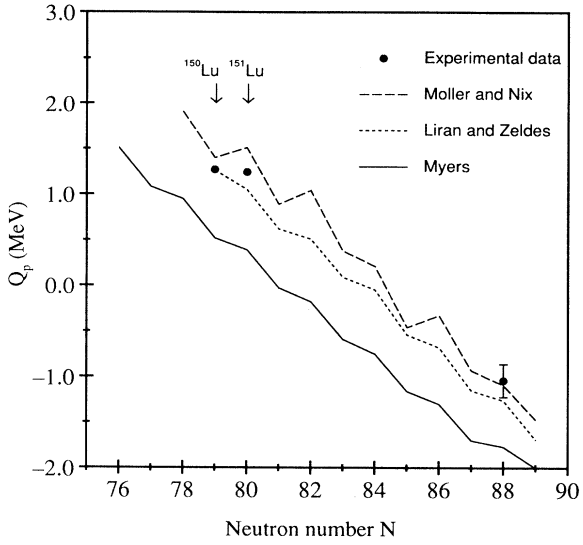

FIG. 10. Proton Q values for isotopes of lutetium with calculated values from the mass models of Möller and Nix, Liran and Zeldes, and Myers. The two proton decay data points from ^{150}Lu and ^{151}Lu are shown (error bars are smaller than the symbol size).

VI. SUMMARY

The explicit mass assignment provided by the Daresbury recoil separator has enabled direct proton transitions from ^{147}Tm, ^{150}Lu, and ^{151}Lu to be unambiguously identified. The high correlation efficiency provided by the double-sided strip detector allows the half-life measurement of weak proton transitions and five new values are reported. These include the first half-life measurement of the proton decay of ^{150}Lu and new half-life measurements for proton transitions from ^{109}I, ^{147}Tm, and ^{151}Lu which are consistent with the previously obtained values and generally have an improved precision. The measured half-lives of these proton emitters around

$A \simeq 150$ give good agreement with calculated estimates, and are consistent with a spherical shell-model description of these nuclei. This is in contrast to the proton transitions observed from the deformed nuclei ^{109}I and ^{113}Cs, which cannot be described in terms of pure shell-model states. Further proton radioactivity measurements linking these two regions are clearly desirable to understand in more detail the factors influencing proton decay transition probabilities.

This work was supported by the U.K. Science and Engineering Research Council. We would like to thank the crews at the NSF for providing the beams.

[1] S. Hofmann, W. Reisdorf, G. Münzenberg, F. P. Hessberger, J. R. H. Schneider, and P. Armbruster, Z. Phys. A **305**, 111 (1982).
[2] O. Klepper, T. Batsch, S. Hofmann, R. Kirchner, W. Kurcewicz, W. Reisdorf, E. Roeckl, D. Schardt, and G. Nyman, Z. Phys. A **305**, 125 (1982).
[3] T. Faestermann, A. Gillitzer, K. Hartel, P. Kienle, and E. Nolte, Phys. Lett. **137B**, 23 (1984).
[4] A. Gillitzer, T. Faestermann, K. Hartel, P. Kienle, and E. Nolte, Z. Phys. A **326**, 107 (1987).
[5] S. Hofmann, in *Particle Emission from Nuclei,* edited by M. Ivascu and D. N. Poenaru (CRC, Boca Raton, Florida, 1989).
[6] P. J. Sellin, P. J. Woods, D. Branford, T. Davinson, N. J. Davis, D. G. Ireland, K. Livingston, R. D. Page, A. C. Shotter, S. Hofmann, R. A. Hunt, A. N. James, M. A. C. Hotchkis, M. A. Freer, and S. L. Thomas, Nucl. Instrum. Methods A **311**, 217 (1992).
[7] P. J. Sellin, Ph.D. thesis, University of Edinburgh, 1992.
[8] S. Hoffman, Y. K. Agarwal, P. Armbruster, F. P. Hessberger, P. O. Larsson, G. Münzenberg, K. Poppensieker, W. Reisdorf, J. R. H. Schneider, and H. J. Schött, in *Proceedings of the 7th International Conference on Atomic Masses and Fundamental Constants, AMCO-7 Darmstadt, 1984,* edited by O. Klepper (THD, Schriftenreiche Wissenschaft und Technik, Darmstadt, 1984), Vol. 26, p. 184.
[9] P. Möller and J. R. Nix, Atomic Data Nucl. Data Tables **39**, 214 (1988).
[10] S. Hofmann, Kerntechnik **42**, 157 (1983).
[11] S. Hofmann (unpublished).
[12] R. D. Page, P. J. Woods, R. A. Cunningham, T. Davinson, N. J. Davis, S. Hofmann, A. N. James, K. Livingston, P. J. Sellin, and A. C. Shotter, Phys. Rev. Lett. **68**, 1287 (1992).
[13] A. Rytz, At. Data Nucl. Data Tables **47**, 205 (1991).
[14] S. Hofmann, G. Münzenberg, K. Valli, F. Hessberger, J. R. H. Schneider, P. Armbruster, B. Thuma, and Y. Eyal, GSI Report No. GSI-82-1, 1982, p. 241.
[15] P. O. Larsson, T. Batsch, R. Kirchner, O. Klepper, W. Kurcewicz, E. Roeckl, D. Schardt, W. F. Feix, G. Nyman, and P. Tidemand-Petersson, Z. Phys. A **314**, 9 (1983).
[16] R. Broda, P. J. Daly, J. H. McNeill, Z. W. Grabowski, R. V. F. Janssens, R. D. Lawson, and D. C. Radford, Z. Phys. A **334**, 11 (1989).
[17] H. Heine, T. Faestermann, A. Gillitzer, J. Homolka, M. Köpf, and W. Wagner, Z. Phys. A **340**, 225 (1991).
[18] F. D. Becchetti and G. W. Greenlees, Phys. Rev. **182**, 1190 (1969).
[19] F. G. Perey, Phys. Rev. **131**, 745 (1963).
[20] K. S. Toth, J. M. Nitschke, P. A. Wilmarth, Y. A. Ellis-Akovali, D. C. Sousa, K. Vierinen, D. M. Moltz, J. Gilat, and N. M. Rao, in *Nuclei Far from Stability,* Proceedings of the 5th International Conference on Nuclei Far from Stability, AIP Conf. Proc. No. 164, edited by Ian S. Towner (AIP, New York, 1987), p. 718.
[21] M. O. Kortelahti, K. S. Toth, K. S. Vierinen, J. M. Nitschke, P. A. Wilmarth, R. B. Firestone, R. M. Chasteler, and A. A. Shihab-Eldin, Phys. Rev. C **39**, 636 (1989).
[22] Y. A. Akovali, K. S. Toth, A. L. Goodman, J. M. Nitschke, P. A. Wilmarth, D. M. Moltz, M. N. Rao, and D. C. Sousa, Phys. Rev. C **41**, 1126 (1990).
[23] K. S. Toth, Y. A. Ellis-Akovali, J. M. Nitschke, P. A. Wilmarth, P. K. Lemmertz, D. M. Moltz, and F. T. Avignone, Phys. Lett. B **178**, 150 (1986).
[24] P. Kleinheinz, B. Rubio, M. Ogawa, M. Piiparinen, A. Płochocki, D. Schardt, R. Barden, O. Klepper, R. Kirchner, and E. Roeckl, Z. Phys. A **323**, 705 (1985).
[25] K. S. Toth, J. Gilat, J. M. Nitschke, P. A. Wilmarth, K. Vierinen, and F. T. Avignone, Phys. Rev. C **36**, 826 (1987).
[26] K. S. Toth, in Proceedings of the 6th International Conference on Nuclei far from Stability, Bernkastel-Kues, 1992 (IOP, Bristol, U.K., in press).
[27] E. Nolte, S. Z. Gui, G. Colombo, G. Korschinek, and K. Eskola, Z. Phys. A **306**, 223 (1982).
[28] K. S. Toth, D. C. Sousa, J. M. Nitschke, and P. Wilmarth, Phys. Rev. C **37**, 1196 (1988).
[29] K. S. Toth, D. C. Sousa, J. M. Nitschke, and P. A. Wilmarth, Phys. Rev. C **35**, 620 (1987).
[30] J. M. Nitschke, P. A. Wilmarth, J. Gilat, K. S. Toth, and F. T. Avignone, Phys. Rev. C **37**, 2694 (1988).
[31] K. Takahashi, M. Yamada, and T. Kondoh, At. Data Nucl. Data Tables **12**, 101 (1973).
[32] K.-N. Huang, M. Aoyagi, M. H. Chen, B. Crasemann, and H. Mark, At. Data Nucl. Data Tables **18**, 243 (1976).
[33] R. D. Page, Ph.D. thesis, University of Birmingham, 1990.
[34] C. M. Perey and F. G. Perey, Nucl. Data Tables **10**, 539 (1972).
[35] V. P. Bugrov and S. G. Kadmenskiĭ, Yad. Fiz. **49**, 1562 (1989) [Sov. J. Nucl. Phys. **49**, 967 (1989)].
[36] R. Bengtsson, P. Möller, J. R. Nix, and Jing-ye Zhang, Phys. Scr. **29**, 402 (1984).
[37] S. Liran and N. Zeldes, At. Data Nucl. Data Tables **17**, 431 (1976).
[38] W. D. Myers, Nucl. Phys. **A415**, 387 (1970).
[39] S. Hofmann, G. Münzenberg, W. Faust, H. Hessberger, W. Reisdorf, J. R. H. Schneider, P. Armbruster, K. Güttner, and B. Thuma, in Proceedings of the 4th International Conference on Nuclei far from Stability, Helsingør, 1981, edited by L. O. Skolen (CERN Report 81-09, 1981), p. 190.

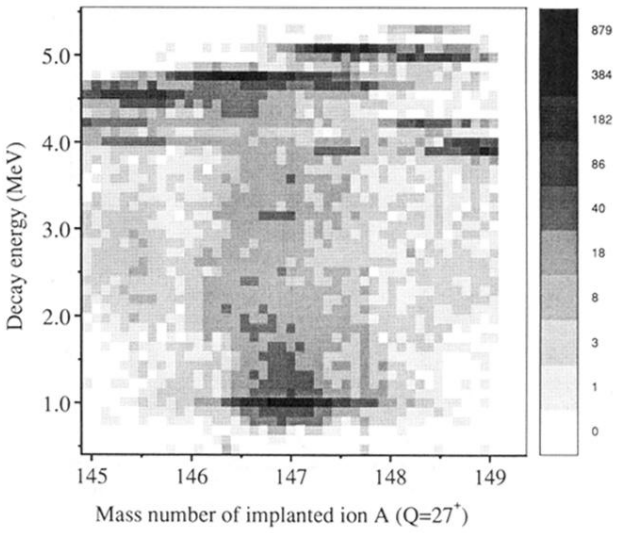

FIG. 2. Plot of decay energy vs mass number of the implanted ion, for events from $^{150}Yb^{*}$. The two proton peaks are contained within the low-energy line in mass group $A = 147$.